Simulation of a Photovoltaic-Thermal (PV-T) Air Source Heat Pump (ASHP) System for Building Thermal Demands

Pranay Kasturi[1,2], Dr. Herena Torio[2,3] and Jan Sören Schwarz[1,2]

[1] OFFIS Institute for Information Technology, Oldenburg (Germany)

[2] University of Oldenburg, Oldenburg (Germany)

[3] DLR Institute of Networked Energy Systems, Oldenburg (Germany)

Abstract

The coupling of photovoltaic-thermal (PV-T) collectors with heat pumps improves both the electrical and thermal performance of the heat pumps. The main objective of this study is to investigate the potential efficiency improvements resulting from the combined operation of an air PV-T system with an air source heat pump (ASHP). We simulate the said combined operation of the system for meeting building thermal demands (space heating and domestic hot water production), using models developed for this study. Different configurations of the PV-T collector system (from 2 to 12 panels in series) are simulated, and the configuration with 4 panels in series is identified as the most suitable one in this context. This configuration of the PV-T ASHP system has better electrical performance as compared to the baseline case of only a photovoltaic (PV) ASHP system with the same configuration, with a 6.61% increase in the seasonal COP of the heat pump. The presented simulation methodology builds the base for further investigation of other types of PV-T collector systems and heat pumps.

Keywords: Heat pumps, PV-T collectors, co-simulation, open-source modelling, Python

1. Introduction

Heat pumps will play a crucial role in reducing the carbon emissions of the buildings sector, as they provide the largest electrification opportunity, displacing heating from fossil fuel boilers (Cozzi and Gould, 2021). Coupling the heat pumps with renewable energy sources will be critical for decarbonization. In this context, photovoltaic thermal (PV-T) collectors are increasingly being used to assist the heat pumps. In addition to generating electrical energy that can be self-consumed, the PV-T collectors also generate thermal energy that can be used as a heat source for the heat pump, resulting in higher source temperatures, and thereby higher efficiency, enhancing the decarbonization potential and grid-friendly operation of heat pumps. The main objective of this study is to investigate the efficiency improvements resulting from the coupling of air PV-T systems with air-source heat pumps (ASHP). For this, we simulate the combined operation of PV-T and ASHP systems for building thermal demands (space heating and domestic hot water production) and compare its performance with a reference case consisting of a photovoltaic (PV) system coupled with an ASHP system. Based on the results, we identify the optimal size of the PV-T system for the demands in consideration and evaluate the benefits that can be achieved with the said combined operation.

2. Methodology

2.1 Basis for the scenario simulations

The basis for the system simulations is the building thermal demand, available as separate profiles for space heating and domestic hot water, for two buildings from the Energetisches Nachbarschafts-Quartier (ENaQ) project (WWW1), for the year 2020. The total annual domestic hot water and space heating demands are 73081 kWh and 35921 kWh respectively. The heating system configuration for the baseline scenario consists of an ASHP, coupled with a hot water tank between the ASHP and the consumer. For the PV-T ASHP system, an indirect expansion

Selection and/or peer review under responsibility of Scientific Committee
10.18086/eurosun.2024.02.09 Available at http://proceedings.ises.org

configuration is chosen, with an air PV-T collector system added in parallel to the external air source of the baseline scenario configuration. The proposed system schematic is shown in the figure 1. In the cases where the demand cannot be met by the system, back up electrical heaters are considered to supply the demands.

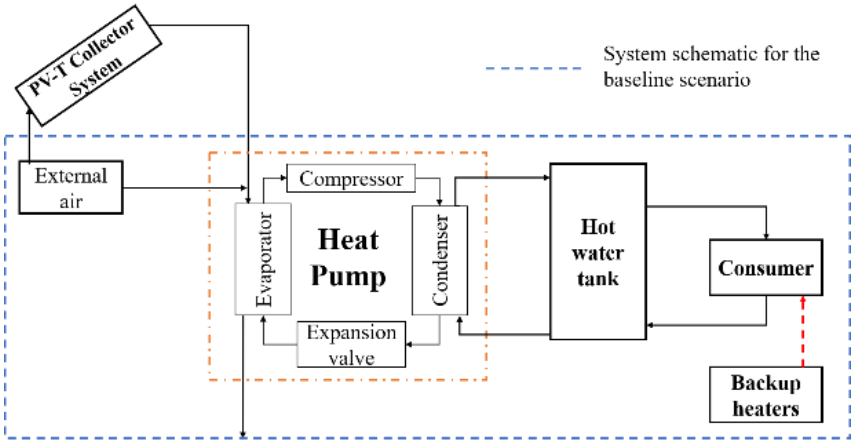

Figure 1: Proposed schematic for the heating system

System design data, shown in table 1, has been obtained from project planning of the energy cooperative Olegeno (WWW2). The weather data required for the simulations has been obtained from PVGIS (WWW3) for the year 2020. The temperature of the cold water replacing the domestic hot water in the tank is also necessary for the simulations, and is assumed to follow a sinusoidal curve (Heimrath, 2004).

Table 1: System design parameters

System Design Parameter	Value
Total peak heating demand (kW)	58
Total volume of hot water storage (Litres)	4000
Space heating supply temperature (°C)	35
Space heating circuit temperature drop (°C)	7
Domestic hot water supply temperature (°C)	40
Total building roof area (m^2)	642

2.2 Models used in the simulations

The different models required for the study have been developed in the Python programming language. The models for the heat pump, hot water tank and the controller, are available as a part of the *mosaik-heatpump* Python package (WWW4). These three models, first developed for a previous work (Barsanti et al., 2021), have been significantly extended for this study. The models are briefly described in this section and detailed documentation of the functionality of these models is available online (WWW5). Additionally, the PV-T system model has been developed for this work and the functionality of this model is described in this section as well.

Heat Pump Model

The combined operation of the PV-T and heat pump systems, lead to higher source temperatures for the heat pump, and therefore lower temperature lift conditions. The performance of heat pumps at such conditions is not trivial. Extrapolating the performance from the standard operation range in the data sheets, as done by simple parametric-fit equation-based models, may lead to errors in the calculated performance (Gasser et al., 2017). Thus, for this work, a detailed quasi-steady state modelling approach has been adopted based on the openly available TESPy library (Witte and Tuschy, 2020).

The performance of the heat pump is simulated by considering the energy and mass balances in the individual *components* of the heat pump – condenser, evaporator, compressor, expansion valve, heat exchangers and pumps

– and the state of fluids in the *connections* between these *components*. The *connections* and *components* together form a topological *network* that is represented and solved as a system of equations. The model is parametrized for the study based on an actual heat pump available in the market, the LW 300L heat pump from ait-deutschland (WWW6), due to its suitability to meet the peak demands mentioned in table 1. The operating conditions, i.e. source air temperature and the condenser water inlet temperature, are provided as inputs to the model. The model then provides the heating capacity, the electrical power consumption, the coefficient of performance (COP), the mass flowrate of water in the condenser and the condenser water outlet temperature as the outputs. The different steps taken to develop the heat pump model (shown in figure 2) based on the LW 300L heat pump are detailed below.

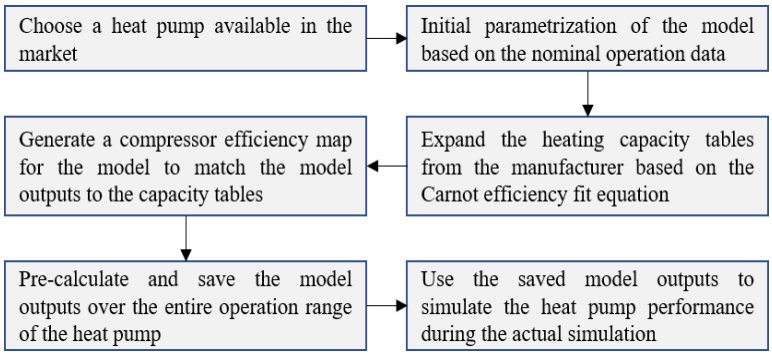

Figure 2: Methodology of heat pump model development

First, an initial calculation of the system network in the *design* calculation mode is performed. The key parameters for the different *components* and *connections* are set based on the nominal operating point data obtained from the manufacturer's datasheet, shown in table 2. All the parameters in the table, except the electrical power, are set as inputs. Since the refrigerant R448A is not available in TESPy, R404A has been used in the model due to the similarity in their properties (Mota-Babiloni et al., 2015). A temperature difference of 5°C is assumed for the water in the condenser. The electrical power consumption of the heat pump is estimated as per the equation 1, where P is the power consumption of the compressor, $\dot{m}_{in}$ is the mass flow in the compressor, $(h_{out,s} - h_{in})$ is the enthalpy change in an isentropic compression process, and η_s is the isentropic efficiency of the compressor. For given operating conditions, η_s is the parameter that affects the power consumption the most and has to be set as an input. Since this value is not available in the datasheet, it is changed on a trial-and-error basis to match the power consumption calculated by the model to that from the datasheet.

$$P = \frac{\dot{m}_{in} \cdot (h_{out,s} - h_{in})}{\eta_s} \qquad \text{(eq. 1)}$$

Table 2: Nominal operating point data of the heat pump

Parameter	Value	Units
Condenser outlet temperature	35	°C
Source air temperature	7	°C
Mass flow of air in evaporator	7800	m^3/h
Heating capacity	32.5	kW
Electrical Power	8.56	kW
Refrigerant	R448A	-

While the initial *design* mode calculation is only for the nominal operating point, the actual operational range of the heat pump varies from -20°C to 35°C for the source air, and 15°C to 65°C for the condenser water outlet temperatures, with varying maximum heating capacities and power consumption. The performance of the heat

pump at these other operating conditions is estimated by the *offdesign* calculation mode of TESPy, which uses the initial design calculation along with generic characteristic curves of the components available in the library. Instead of using the generic curve for η_s over the entire operation range, a series of design points (table 3) are identified where the η_s is changed as done in the initial design point calculation explained earlier.

Table 3: Design point conditions

Parameter	Values
Source air temperature (°C)	-20, -15, -12, -10, -7, -2, 2, 7, 10, 12, 15, 20, 25, 30, 35
Condenser outlet temperatures (°C)	15, 20, 25, 30, 35, 40, 45, 50, 55

From the table 3, every pair of source air and condenser water temperatures forms an operating point at which the maximum heating capacity and power consumption are required for the design point calculation. The manufacturer's datasheet contains the respective curves for the entire range of temperatures of source air, but only for two specific condenser water outlet temperatures (35°C & 55°C). Therefore, the maximum heating capacity and power consumption have to be estimated for the missing condenser water outlet temperatures. The maximum heating capacity is strongly influenced only by the source air temperature and the average of the capacities at the two available condenser water outlet temperatures is assumed for all the missing points. The corresponding power consumption, however, is influenced strongly by both the source air temperature as well as the condenser water outlet temperature, and hence has been estimated using an approach based on the Carnot effectiveness fit equation.

For all the operating points at which the power consumption is known, the temperature lift (T_{lift}) and ideal COP (COP_{ideal}) are calculated according to equations 2 & 3 respectively, where T_h is the condenser water outlet temperature and T_c is the source air temperature. The Carnot effectiveness (η_{carnot}) is then calculated according to equation 4, using the real COP of the heat pump (COP_{real}). A second order polynomial equation is fit to the η_{carnot} vs. T_{lift} curve. For the operating points with missing power consumption data, this fit equation is used to estimate the Carnot effectiveness, which in turn is used to estimate the power consumption. The network calculations in the *design* mode are then made for each of the operating points and the compressor isentropic efficiency is changed to match the power consumption calculated by the model with the estimated values, there by generating the so-called compressor efficiency map. The *offdesign* mode with the generic curve for η_s is then used only in the smaller ranges between the different design points.

$$T_{lift} = T_h - T_c \qquad \text{(eq. 2)}$$

$$COP_{ideal} = \frac{T_h}{T_h - T_c} \qquad \text{(eq. 3)}$$

$$\eta_{carnot} = \frac{COP_{real}}{COP_{ideal}} \qquad \text{(eq. 4)}$$

The model is then finally developed to estimate the heat pump performance over the entire operation range, with a 1°C resolution for both the inputs of the model, the source air and condenser water inlet temperatures. For each set of inputs, assuming a rise of 5°C for the water in the condenser, the model identifies the closest design point, and first runs the design point calculation using the respective values for the maximum heating capacity and η_s from the map. The model then uses the *offdesign* calculation mode to estimate the performance at the input conditions, assuming the same heating capacity as in the design point and using the generic curve for η_s. The condenser water outlet temperature, the mass flow rate of water, the power consumption and the COP of the heat pump, are all calculated by the model and provided as outputs. The inputs and corresponding outputs of the model are saved. During the scenario simulations, the saved inputs that are closest to the input data are identified, and the saved output data for these points are used to calculate the outputs of the model, rather than performing the actual *design* and *off-design* calculations. Though the granularity of the model is reduced, there is a significant improvement in the simulation duration.

PV-T collector system model

The PV-T collector system model has been developed as a combination of two separate models for the thermal and photovoltaic components of the collector, once again following a quasi-steady state modelling approach. The tilted plane irradiance (E) and the temperature of the air at the inlet of the PV-T field, which is the same as the ambient temperature (T_{amb}), are provided as inputs to the model. The outlet temperature of air from the PV-T field which is used as the source air in the heat pump, and also the electricity generated by the PV-T field which can be self-consumed by the heat pump, are calculated as the outputs of the model.

The thermal performance has been modelled based on the solar collector component available in the TESPy library. The equations for steady state energy balance (equations 5 & 6) are applied to each collector panel, where ($h_{out} - h_{in}$) is the enthalpy change of the fluid in the collector and T_m is the mean temperature of the fluid in the collector panel. The inlet temperature for each panel (T_{in}), T_{amb} and E are provided as inputs, to calculate the temperature of the fluid in the outlet *connection* (T_{out}) of the panel. While T_{amb} is used as the T_{in} for the first panel in series, the T_{out} from the previous panel is used as the T_{in} for the next panel in series. The relevant parameters - collector area (A), optical efficiency (η_{opt}), linear thermal loss coefficient (α_1), quadratic thermal loss coefficient (α_2), and mass flow of air ($\dot{m}$)- have been obtained from literature for a reference glazed type PV-T air collector (Tonui and Tripanagnostopoulos, 2007), and are summarized in table 4. The outlet temperature from the final panel is series is used as the source air temperature in the heat pump. A mixing strategy has been implemented to ensure that this temperature is within the limits of operation of the heat pump. The temperature of the source air in the heat pump should be lower than both the maximum temperature limit (35°C) and the condenser water inlet temperature of the heat pump. In case the outlet temperature of air from the PV-T system is higher than either of these, the outlet air is mixed with ambient air to bring down the temperature to the lower value of the two.

$$\dot{m} * (h_{out} - h_{in}) = A * (E * \eta_{opt} - \alpha_1 * (T_m - T_{amb}) - \alpha_2 * (T_m - T_{amb})^2 \quad \text{(eq. 5)}$$

$$T_m = \frac{T_{out} + T_{in}}{2} \quad \text{(eq. 6)}$$

Table 4: Thermal parameters of the collector

Parameter	Value	Units
Operating fluid	Air	
$\dot{m}$	0.02	kg/s
A	0.4	m^2
η_{opt}	0.364	-
α_1	4.79	W/K-m^2
α_2	0	W/K^2-m^2

The PV performance has been modelled as a standalone PV panel, considering just the effect of panel temperature on its efficiency. The electrical power output of the PV module (P) is calculated using eq. 7. The electrical efficiency (η_{el}) of the collector varies with the temperature of the PV module (T_{PV}) and is calculated as shown in eq. 8, where the reference electrical efficiency ($\eta_{el,ref}$) at standard test conditions (STC – 25°C) and the temperature coefficient (β_0) have been obtained from literature for a reference glazed type PV-T air collector (Tonui and Tripanagnostopoulos, 2007), and are shown in table 5.

$$P = \eta_{el} * E * A \quad \text{(eq. 7)}$$

$$\eta_{el} = \eta_{el,ref} * (1 - \beta_0 * (T_{PV} - 25)) * E * A \quad \text{(eq. 8)}$$

When the thermal component of the PV-T collector was being operated, to supply air to the heat pump, the temperature of the PV module (T_{PV}) is assumed to be the mean temperature of the air inside the collector (Kramer, 2020), as calculated by eq. 6. For the systems with multiple collector panels in series, the mean temperature in each

panel varies, leading to a varying production of electricity.

Table 5: Photovoltaic parameters of the PV-T collector

Parameter	Value	Units
$\eta_{el,ref}$	0.13	-
β_0	0.006	1/K
$T_{PV,NOCT}$	43	^{0}C
$T_{amb,NOCT}$	20	^{0}C
E_{NOCT}	800	W/m^2
$T_{PV,ref}$	25	^{0}C
$\tau\alpha$	0.83	-

However, in the cases when the heat pump is turned off, the thermal component of the PV-T collector is not operated, and the temperature of the PV module is calculated using the PV cell temperature equation available in the HOMER simulation software (WWW7), as shown in eq. 9. $T_{PV,NOCT}$ is the nominal operating cell (PV module) temperature (NOCT), $T_{amb,NOCT}$ is the ambient temperature at NOCT, E_{NOCT} is the tilted plane irradiance at NOCT, $T_{PV,ref}$ is the PV module temperature at the reference STC conditions, τ and α are the solar transmittance and the solar absorptance of the PV module. All of these parameters have also been obtained from literature for a reference glazed type PV-T air collector (Tonui and Tripanagnostopoulos, 2007), and are summarized in table 5. All the temperatures have been converted to the Kelvin scale before being used in the equation. In these cases, the electricity generated by all the individual panels in the system is assumed to be the same. The electricity generation of only the PV system, is also estimated using the same equations (7 & 8), with the cell temperature always calculated using the eq. 9.

$$T_{PV} = \frac{T_{amb}+\left(T_{PV,NOCT}-T_{amb,NOCT}\right)*\left(\frac{E}{E_{NOCT}}\right)*\left(1-\frac{\eta_{el,ref}*(1-\beta_0*T_{PV,ref})}{\tau\alpha}\right)}{1+\left(T_{PV,NOCT}-T_{amb,NOCT}\right)*\left(\frac{E}{E_{NOCT}}\right)*\left(\frac{\beta_0*T_{PV,ref}}{\tau\alpha}\right)} \qquad \text{(eq. 9)}$$

For the PV-T collector field, the number of panels in parallel are calculated to be 133, considering the need to maintain a fixed mass flow rate within each panel (0.02 kg/s) and to supply the required mass flow of air to the heat pump (2.65 kg/s). Each of the 133 strings can have a maximum of 12 panels in series, considering the panel area of 0.4 m^2 (from table 1) and the available building roof area of 642 m^2, as mentioned in section 2.1.

Hot water tank model

The hot water tank model developed for another project (Gerster et al., 2016), is used in this work to act as a buffer in between the heating device and the heat consumer. It is a multinode stratified thermal tank model (Saloux and Candanedo, 2019), where the tank volume is divided into a specified number of layers (nodes) of equal volume, each characterized by a specific temperature. A traditional density distribution approach is adopted where the water flowing into the tank enters the layer that best matches its density (i.e., temperature). The model assumes that the fluid streams are fully mixed before leaving each of the layers and the flows between the layers follow the law of mass conservation. Heat transfer to the surrounding environment from the walls of the tank, and the heat transfer between the layers have been considered.

The schematic of the hot water tank model is shown in figure 3. The dimensions of the tank are specified in terms of its volume and height. The storage volume required is 4000L (table 1). The height of the tank is calculated assuming a height to diameter ratio of 3:1. Based on the literature for the optimum number of nodes in the tank (Saloux and Candanedo, 2019), especially its impact on long term simulations (Arias et al., 2008), the tank is parametrized to contain six layers. The initial temperature of all the layers at the beginning of the simulation is set to 20°C.

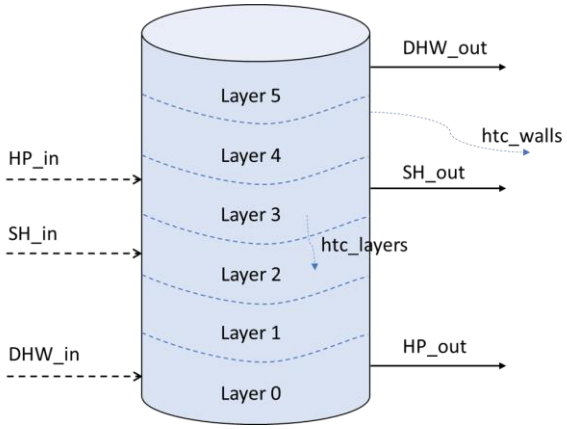

Figure 3: Schematic representation of the hot water tank model

The flows into and out of the tank are specified as the connections of the hot water tank model. The flow going to the heat pump (*HP_out*), the space heating demand (*SH_out*), and the domestic hot water demand (*DHW_out*) are connected to the bottom layer, the fourth layer and the top layer respectively. As described above, the corresponding flows coming into the tank (*HP_in*, *SH_in*, and *DHW_in*) are not connected to a fixed layer in the tank. They are connected to the layer with a temperature closest to that of the flow. The heat transfer coefficient of the walls of the tank (*htc_walls*) is assumed to be 0.28 W/m^2 - K (Heimrath, 2004). The heat transfer coefficient for the heat transfer between the layers of the tank (*htc_layers*) is assumed to be 1.5 times the thermal conductivity of water (Heimrath, 2004). The value is calculated as 0.897 W/m-K, considering the thermal conductivity of water to be 0.598 W/m-K (WWW8).

Controller model

The controller model used in this work utilizes simple Boolean logic to match the heating demands with the supply from the hot water tank/back up heaters. The controller is initialized with the set points mentioned in table 1. Based on the heat demands, the controller calculates the necessary mass flows for the hot water tank model. For the domestic hot water demand, the supplied water is replaced by the cold water. Additionally, if the supply temperature is higher than the set point, the flow is adjusted by mixing with the cold water to bring the temperature down to the set point. For the space heating demand a constant temperature drop of 7°C in the circuit is assumed. For both the demands, if the supply temperatures are lower than the set points, the controller calculates the additional heat that must be supplied by the backup heaters, assuming 100% efficiency for the heaters.

The controller model also controls the operation of the heat pump with a control strategy based on the temperatures of both the bottom and top layers of the tank. The fifth layer of the hot water tank is considered as the top layer instead of the sixth layer, in order to ensure a higher temperature in the actual top layer for periods of high demands. The top layer of the tank is controlled against the higher set point of 43°C, i.e., the heat pump is turned on when the temperature in the top layer of the tank falls below the higher set point. The bottom layer of the tank is controlled against the lower set point of 37°C, i.e., the heat pump is turned off only when the temperature in the bottom layer of the tank is greater than the lower set point. In this case, the temperature of the top layer is expected to be greater than the higher set point due to stratification inside the tank. The heat pump continues to remain turned off and turns back on only when the temperature of the top layer falls below the higher set point again.

The controller model can also adapt the control strategy during the photovoltaic-thermal (PV-T) collector operation. When operating the photovoltaic-thermal (PV-T) collector along with the heat pump, an advanced control strategy has been implemented in an attempt to extend the operation of the heat pump during the daytime when the source air for the heat pump is available at a higher temperature. The set points for the heat pump operation are increased by the value of the temperature difference of the air inside the PV-T system. This increase is limited to a maximum of 7°C, in order to not heat up the tank much higher than that required for the domestic hot water supply.

2.3 Co-simulation

The stand-alone models for heat pump, hot water tank, photovoltaic thermal (PV-T) system and controller are dependent on the information from each other that only becomes available over the course of the simulation, as shown in figure 4. This type of joint simulation of models is called co-simulation. In this work, the co-simulation framework mosaik (Steinbrink et al., 2019) has been used to couple the independent models. The models have been implemented with the mosaik component application programming interface (API) to allow coupling with mosaik. Additionally, the scenario API provided by mosaik has been used to specify data flows between the coupled models in the scenario definition and execute the co-simulation. The input and output data for all the models is handled by mosaik-csv (WWW9), a tool available in mosaik that operates as a pseudo simulator to handle data in the CSV (comma separated values) data format. The co-simulation of all the models is done at a time step of 1 minute, with the information being exchanged between all the models after each time step of the simulation.

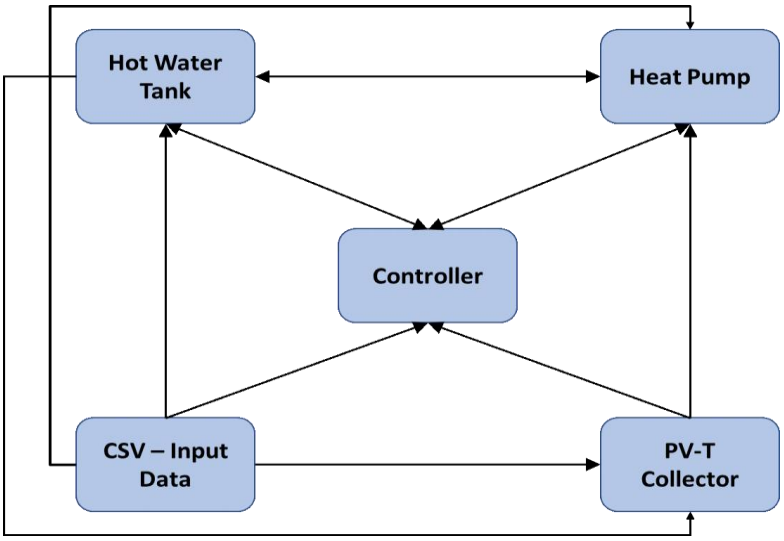

Figure 4: The flow of information between the different models

2.4 Scenarios

The system simulations are performed for the PV-T ASHP system, for a range of configurations of the PV-T field, with 2,4,6,8,10 and 12 PV-T collector panels connected in series, limited by the roof area available as explained earlier. The system performance for the different configurations are compared to the baseline of PV ASHP system with corresponding configurations of the PV field. The annual energy supply, seasonal COP of the heat pump, self-consumption of electrical energy by the heat pump, and grid electrical energy consumed by the system are used as indicators for the system performance comparison. Based on the comparison, the PV-T collector field configuration that is most appropriate for the building thermal demands in consideration is identified. This configuration of the PV-T ASHP system is finally simulated with the advanced control strategy described earlier.

3. Results

The simulations are performed for all the scenarios described in section 2.4 and the performance of the system is evaluated using the key performance indicators (KPIs) shown in table 6. While the results for only two configurations of the PV-T/PV field (4 and 12 panels in series) of both the PV-T ASHP and PV ASHP systems are shown in the table, additional plots with results from the simulations of the other configurations are also shown and discussed in section 3.1. The configuration with 4 panels in series is identified as the optimal one for the thermal demands in consideration and is simulated with the advanced control strategy described in the ‘Controller model’ part of section 2.2. The performance of the system from this simulation is evaluated again using the same KPIs, as shown in the table 6, and the results are discussed with an additional plot in section 3.2.

Table 6: Comparison of KPIs for different configurations of PV-T/PV ASHP Systems (annual for 2020) (TE- thermal energy; EE- electrical energy; HP- heat pump; HWT- hot water tank; ACS – advanced control strategy)

System configuration / System performance KPIs	PV ASHP	PV-T ASHP	PV ASHP	PV-T ASHP	PV-T ASHP	Units
	4 panels in series		12 panels in series		ACS	
TE - system (kWh)	110221.04	110223.50	110221.04	110218.41	110326.79	kWh
EE - system (kWh)	31476.52	29534.94	31476.52	28358.63	30035.28	kWh
EE - HP (kWh)	30779.48	28883.05	30779.48	27638.69	29497.40	kWh
TE/EE - backup heaters (kWh)	697.03	651.88	697.03	719.93	537.87	kWh
HWT mean temperature (°C)	40.47	40.52	40.47	40.40	43.12	°C
HP seasonal COP	3.56	3.79	3.56	3.96	3.72	-
PV/-T EE generation (kWh)	35162.48	35548.81	105487.45	104885.85	35613.28	kWh
PV/-T EE self-consumption (kWh)	10367.27	8684.37	15142.88	12045.50	10331.44	kWh
EE from grid (kWh)	21109.24	20850.56	16333.64	16313.13	19703.83	kWh

3.1 Performance evaluation of the system with different configurations of PV/-T field

As seen from the table 6, the total thermal energy for all the cases is almost the same and the thermal energy supplied by the backup heaters is significantly lower with a maximum share of 0.65% of the total thermal energy observed for the '12 panels in series' configuration of the PV-T system. The thermal energy is mostly supplied by the heat pump and consequently most of the electrical energy consumed by the system is that of the heat pump. For the PV-T ASHP system, having higher number of panels in series results in higher temperatures for the source air of the heat pump and therefore results in lower electrical energy consumption/higher COP. However, these KPIs remain same for the PV ASHP system irrespective of the number of panels in series, as the source air for the heat pump is available just at the ambient temperature, as can be seen from table 6.

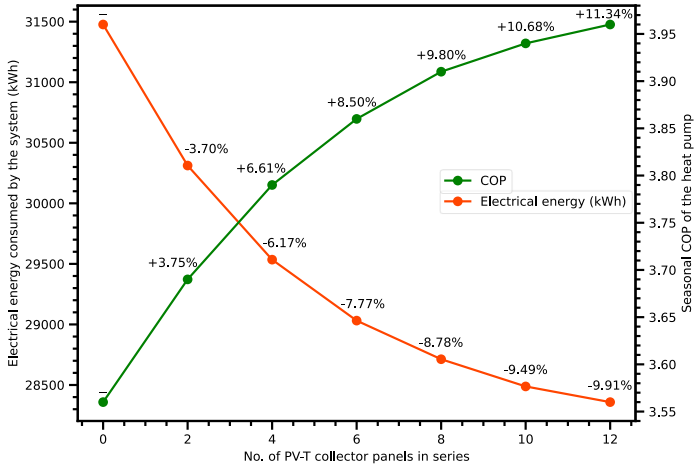

Figure 5: Comparison of system electrical performance for the different configurations of the PV-T collector system

Figure 5 shows the comparison of the electrical performance of all the configurations of the PV-T ASHP system and the PV ASHP system (labelled 0 panels). With an increase in the number of panels in series, the rate of increase/decrease in the COP/total electrical energy consumed reduces. For the PV-T system with 4 panels in series, the COP increases by 6.61%, and by increasing the number of panels in series to 12, the COP is improved further only by an additional 4.73%. As expected, a similar trend can also be seen for the electrical energy consumed by the system. Considering these trends, the PV-T ASHP system configuration with 4 panels in series

for the PV-T field, is identified as the most suitable one for the building thermal demands in consideration.

The electrical energy generated by the PV-T or the PV field, the self-consumption of this electrical energy by the system and the additional electrical energy required from the grid, are influenced by the number of panels in series as can be seen from table 6. For the '4 panels in series' configuration, the total electrical energy generated by the PV-T system is higher than the energy generated by the corresponding PV system, as the heat extracted by the PV-T collector reduces the cell temperature, thereby increasing the electrical efficiency of the PV-T system. However, for the '12 panels in series' configuration, the total electrical energy generated by the PV-T system is lower than that of the corresponding PV system, due to the very high temperatures reached inside the panels which reduce the electrical efficiency.

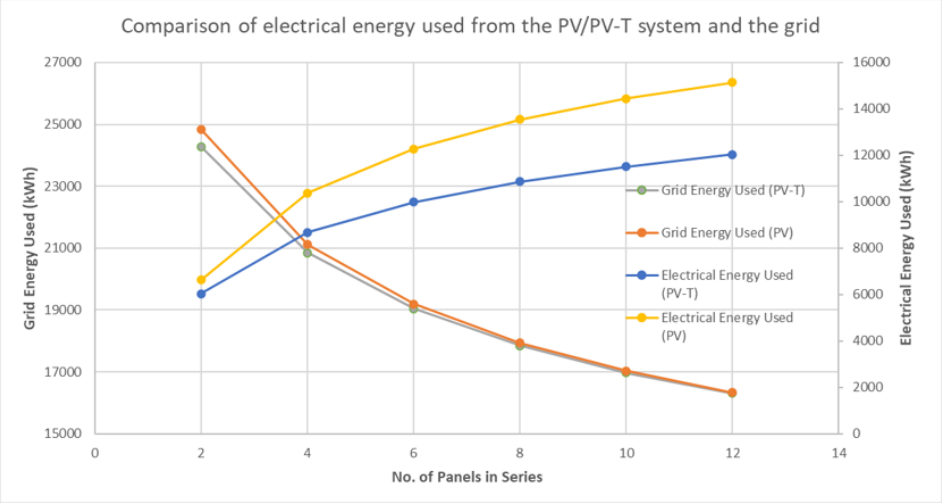

Figure 6: Comparison of the electrical energy used from the PV/PV-T field and the grid for different configurations of PV/PV-T field

Figure 6 shows the comparison of the self-consumption of electrical energy generated by the PV-T/PV field and the electrical energy from the grid, for all the configurations simulated. The self-consumption of electrical energy generated by the PV-T ASHP system is always lower than that of the PV ASHP system, due to the lower operation duration of the PV-T ASHP system as a result of the higher heating capacities of the heat pump at the higher source air temperatures. However, due to lower total electrical energy consumption by the PV-T ASHP system, the grid energy used is lower than that used by the PV ASHP system for all the configurations.

3.2 Advanced control strategy

The configuration of the PV-T collector with 4 panels in series, which has been identified as the most suitable one for the building thermal demands, has been simulated with the advanced control strategy which extends the operation of the system during the daytime by increasing the control set points for the hot water tank. This is reflected in the higher HWT mean temperature of 43.12°C as can be seen in table 6. The total electrical energy consumed by the system, and that consumed by the heat pump increase by 1.7% (500 kWh) and 2.1% respectively, with the COP of the heat pump decreasing by 1.9%. This happens due to the higher temperatures in the condenser of the heat pump, with the increase in the temperatures inside the hot water tank at higher control limits. At the same time, the self-consumption of the electrical energy generated by the PV-T system increases by 19% (1647 kWh), due to the synchronised operation of the heat pump and the PV-T system, resulting in a 5.5% (1100 kWh) reduction in the grid electrical energy used.

In order to study the effect of the advanced control strategy, the performance of the system is observed over a shorter time frame of a week in August with high irradiance, as shown in figure 7. The results from the case with the normal control strategy are shown on the left and the results from the case with the advanced control strategy are shown on the right. The temperature of the air at the inlet and the outlet of the PV-T system, labelled '*Air – PV-T inlet*' and '*Air - PV-T outlet*' respectively, the source air temperature for the heat pump, labelled '*Air – HP*

inlet', temperatures of the top and the bottom layers of the hot water tank, labelled '*HWT – Top layer*' and '*HWT – Bottom layer*' respectively, and the heat supplied by the heat pump during day time and night time, labelled '*HP Heat Supply – Day*' and '*HP Heat Supply – Night*' respectively, are shown.

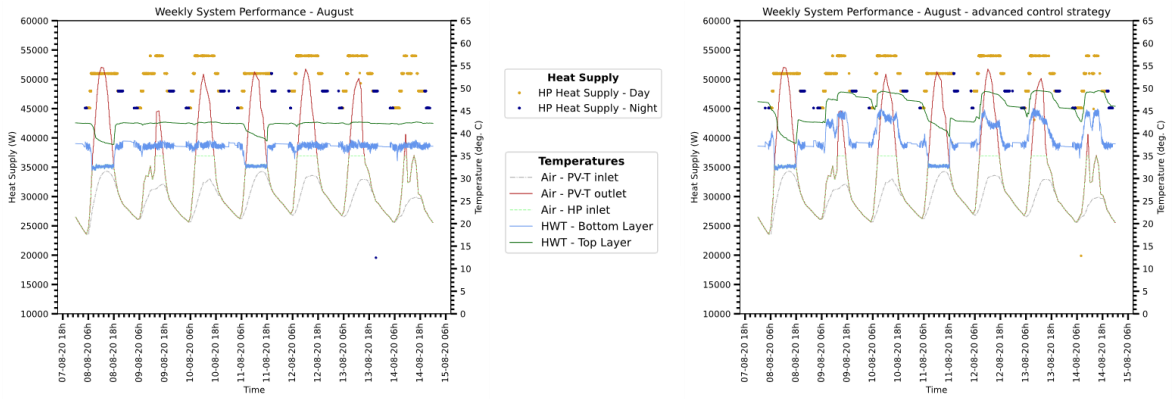

Figure 7: Weekly analysis of the PV-T ASHP system – normal vs advanced control strategy

In the plots on the right-hand side, the increase in the hot water tank temperatures, as compared to the corresponding plot on the left, can be seen during the day time operation of the heat pump. The temperatures for the '*HWT – Top layer*' reach around 50°C in the plot on the right, and is limited to less than 43°C in the plot on the left. It can be observed from both the plots that the '*Air – HP inlet*' is restricted to the heat pump operation limit of 35°C, despite the 'Air – PV-T outlet' temperature being reaching up to 50°C, as a result of the mixing strategy explained in the 'PV-T collector system model' part in section 2.2. This explains the reducing improvement in the system performance as the number of panels in series in the PV-T field increase beyond 4 panels in series. The PV-T outlet temperatures already breach the temperature limit of operation for the heat pump at time with high irradiance. Thus, with more panels in series, though the PV-T field achieves higher outlet temperatures for air, the heat pump cannot utilize it.

4. Conclusions

PV-T collectors are a suitable low temperature source to increase the performance of a decentralized HP when no other low temperature sources (like waste or geothermal heat) are available. Based on the energy performance analysis the PV-T collector field configuration with 4 panels in series is found to be the most suitable one for the building thermal demands in consideration. This configuration of the PV-T ASHP system has better electrical performance as compared to the PV ASHP system with the same configuration, with a 6.61% increase in COP. Consequently, the PV-T ASHP system has lower grid electrical energy consumption. Though the advanced control strategy resulted in a 1.9% decrease in the COP of the heat pump, an increase of 19% in the self-consumption of the electrical energy generated by the PV-T system resulted in a 5.5% decrease in the grid electrical energy used by the system. While these results show the potential improvement in the system performance that can be achieved by connecting an air PV-T collector system in an indirect expansion configuration with an ASHP system, the presented simulation methodology can be extended to research other types of PV-T collector systems, heat pumps and configurations for combined operation. Furthermore, including an analysis of the costs for investment and operation would shed additional light on the optimal design, sizing and control of such system configurations.

5. Acknowledgments

This research was funded by the Lower Saxony Ministry of Science and Culture under grant number 11-76251-13-3/19–ZN3488 (ZLE) within the Lower Saxony "SPRUNG" of the Volkswagen Foundation. It was supported by the Center for Digital Innovations (ZDIN).

6. References

Arias, D.A., McMahan, A.C., Klein, S.A., 2008. Sensitivity of long-term performance simulations of solar energy systems to the degree of stratification in the thermal storage unit. Int J Energy Res 32, 242–254. https://doi.org/10.1002/ER.1344

Barsanti, M., Schwarz, J.S., Gérard Constantin, L.G., Kasturi, P., Binder, C.R., Lehnhoff, S., 2021. Socio-technical modeling of smart energy systems: a co-simulation design for domestic energy demand. Energy Informatics 4, 1–13. https://doi.org/10.1186/S42162-021-00180-6/TABLES/2

Cozzi, L. (International E.A., Gould, T. (International E.A., 2021. World Energy Outlook 2021 1–386.

Gasser, L., Flück, S., Kleingries, M., Meier, C., Bätschmann, M., Wellig, B., 2017. O.1.4.5 High efficiency heat pumps for low temperature lift applications - HPT - Heat Pumping Technologies, in: 12th IEA Heat Pump Conference.

Gerster, J., Blank, M., Stern, K., Sonnenschein, M., 2016. Intelligentes Heimenergiemanagement – Nutzung der Synergiepotentiale bei der thermischen und elektrischen Objektversorgung durch modellbasierte und prädiktive Betriebsführungsstrategien - Tagungsbeiträge - VDE VERLAG, in: VDE-Kongress 2016 - Internet Der Dinge. VDE VERLAG GMBH, Berlin, Offenbach.

Heimrath, R., 2004. Simulation, Optimierung und Vergleich solarthermischer Anlagen zur Raumwärmeversorgung für Mehrfamilienhäuser. Institut für Wärmetechnik.

Kramer, K., 2020. Status Quo of PVT Characterization. https://doi.org/10.18777/ieashc-task60-2020-0004

Mota-Babiloni, A., Navarro-Esbrí, J., Peris, B., Molés, F., Verdú, G., 2015. Experimental evaluation of R448A as R404A lower-GWP alternative in refrigeration systems. Energy Convers Manag 105, 756–762. https://doi.org/10.1016/J.ENCONMAN.2015.08.034

Saloux, E., Candanedo, J.A., 2019. Modelling stratified thermal energy storage tanks using an advanced flowrate distribution of the received flow. Appl Energy 241, 34–45. https://doi.org/10.1016/J.APENERGY.2019.02.075

Steinbrink, C., Blank-Babazadeh, M., El-Ama, A., Holly, S., Lüers, B., Nebel-Wenner, M., Acosta, R.P.R., Raub, T., Schwarz, J.S., Stark, S., Nieße, A., Lehnhoff, S., 2019. CPES testing with MOSAIK: Co-Simulation planning, execution and analysis. Applied Sciences (Switzerland) 9. https://doi.org/10.3390/APP9050923

Tonui, J.K., Tripanagnostopoulos, Y., 2007. Air-cooled PV/T solar collectors with low cost performance improvements. Solar Energy 81, 498–511. https://doi.org/10.1016/J.SOLENER.2006.08.002

Witte, F., Tuschy, I., 2020. TESPy: Thermal Engineering Systems in Python. J Open Source Softw 5, 2178. https://doi.org/10.21105/JOSS.02178

Web references

WWW1- Projekt – ENaQ – Energetisches Nachbarschaftsquartier Fliegerhorst Oldenburg [WWW Document], n.d. URL https://www.enaq-fliegerhorst.de/teilprojekte/ (accessed 08.18.24).

WWW2- Home | Olegeno Oldenburger Energie-Genossenschaft eG [WWW Document], n.d. URL https://www.olegeno.de/ (accessed 08.18.24).

WWW3- JRC Photovoltaic Geographical Information System (PVGIS) - European Commission [WWW Document], n.d. URL https://re.jrc.ec.europa.eu/pvg_tools/en/tools.html#PVP (accessed 08.18.24).

WWW4- Kasturi, P., Schwarz, J.S., n.d. mosaik-heatpump [WWW Document]. URL https://gitlab.com/mosaik/components/energy/mosaik-heatpump (accessed 08.18.24).

WWW5- mosaik-heatpump — mosaik 3.3.0b1 documentation [WWW Document], n.d. URL https://mosaik.readthedocs.io/en/latest/ecosystem/components/mosaik-heatpump/overview.html (accessed 08.18.24).

WWW6- LW Serie | alpha innotec [WWW Document], n.d. URL https://www.alpha-innotec.com/de/warmepumpen/luft-wasser-warmepumpen/lw-serie (accessed 08.18.24).

WWW7- How HOMER Calculates the PV Cell Temperature [WWW Document], n.d. URL https://www.homerenergy.com/products/pro/docs/3.15/how_homer_calculates_the_pv_cell_temperature.html (accessed 08.18.24).

WWW8- Water - Thermal Conductivity vs. Temperature [WWW Document], n.d. URL https://www.engineeringtoolbox.com/water-liquid-gas-thermal-conductivity-temperature-pressure-d_2012.html (accessed 08.18.24).

WWW9- mosaik / components / data / mosaik-csv · GitLab [WWW Document], n.d. URL https://gitlab.com/mosaik/components/data/mosaik-csv (accessed 08.18.24).